Mechanism of voltage-sensitive fluorescence in a microbial rhodopsin

Dougal Maclaurin[a,1], Veena Venkatachalam[b,1], Hohjai Lee[c], and Adam E. Cohen[a,c,2]

[a]Department of Physics, [b]Graduate Program in Biophysics, and [c]Department of Chemistry and Chemical Biology, Harvard University, Cambridge, MA 02138

Edited by Steven G. Boxer, Stanford University, Stanford, CA, and approved March 4, 2013 (received for review September 12, 2012)

Microbial rhodopsins were recently introduced as genetically encoded fluorescent indicators of membrane voltage. An understanding of the mechanism underlying this function would aid in the design of improved voltage indicators. We asked, what states can the protein adopt, and which states are fluorescent? How does membrane voltage affect the photostationary distribution of states? Here, we present a detailed spectroscopic characterization of Archaerhodopsin 3 (Arch). We performed fluorescence spectroscopy on Arch and its photogenerated intermediates in *Escherichia coli* and in single HEK293 cells under voltage-clamp conditions. These experiments probed the effects of time-dependent illumination and membrane voltage on absorption, fluorescence, membrane current, and membrane capacitance. The fluorescence of Arch arises through a sequential three-photon process. Membrane voltage modulates protonation of the Schiff base in a 13-*cis* photocycle intermediate ($M \rightleftharpoons N$ equilibrium), not in the ground state as previously hypothesized. We present experimental protocols for optimized voltage imaging with Arch, and we discuss strategies for engineering improved rhodopsin-based voltage indicators.

Optical recording of membrane potential promises new insights into the individual and collective dynamics of neurons (1, 2), cardiac cells (3), developing embryos (4), and even microbes (5). Despite decades of effort (2, 6, 7), development of effective voltage indicators remains a challenge. We recently discovered that the endogenous fluorescence of some microbial rhodopsin proteins responds sensitively and quickly to changes in membrane voltage (8, 9). Heterologous expression of Archaerhodopsin 3 (Arch) in cultured neurons enabled robust optical recordings of action potentials using a genetically encoded indicator. However, the mechanisms by which these proteins fluoresced and sensed voltage remained obscure. A detailed photophysical understanding of GFP proved essential to its optimization and diversification (10). Thus, we adopted a similar approach for Arch. The aims of this paper are (*i*) to identify optimal imaging conditions for Arch and (*ii*) to explain how Arch functions as a voltage indicator.

Arch (Uniprot P96787) is a microbial rhodopsin derived from the Dead Sea microorganism *Halorubrum sodomense*. The protein contains seven transmembrane α-helices with the chromophore retinal covalently bound via a Schiff base to a lysine in the protein core. In the wild, Arch serves as a light-driven outward proton pump, capturing solar energy for its host (11). Upon expression in neurons, Arch can act as an optogenetic neural silencer: illumination with green light generates a hyperpolarizing photocurrent, which suppresses neural firing (12).

Illumination with orange or red light excites Arch fluorescence; emission is in the near infrared, peaked at 710 nm (8). Fluorescence is sensitive to membrane voltage; with excitation at 640 nm, fluorescence increased twofold from −150 to +150 mV, with a response time of ∼0.6 ms. However, Arch has two undesirable attributes as a voltage indicator. First, the fluorescence is very dim, requiring intense laser illumination to be detectable. Second, illumination of Arch slightly perturbs the membrane potential: under typical illumination for imaging (640 nm, 230 W/cm^2), Arch generates an outward photocurrent in neurons of 34 ± 7 pA ($n = 7$ cells), which hyperpolarizes the membrane by 6.2 ± 1.1 mV. A mechanistic understanding of Arch could guide efforts to engineer improved performance.

The photocycle of Arch is likely similar to that of its close homolog bacteriorhodopsin (BR) (*SI Appendix*, Fig. S1), which we take as a template. Light-induced isomerization of retinal in BR induces a series of conformational shifts that moves one proton across the membrane. In the ground state (g), the retinal is in an *all-trans* conformation and the Schiff base is protonated. Absorption of a green or yellow photon induces photoisomerization to a 13-*cis* conformation ($g \rightarrow L$), followed by proton transfer from the Schiff base to an acceptor on the extracellular side ($L \rightarrow M_1$). The Schiff base then switches accessibility to the cytoplasmic side ($M_1 \rightarrow M_2$), where a proton donor reprotonates the Schiff base ($M_2 \rightarrow N$). The donor takes up a proton from the cytoplasm and the retinal thermally isomerizes back to *all-trans* ($N \rightarrow O$). Finally, the acceptor releases its proton to the proton-release complex on the extracellular side ($O \rightarrow g$). All photocycle intermediates except for M have overlapping absorption spectra peaked between 550 and 630 nm; due to the deprotonated Schiff base, the M intermediates absorb maximally at 410 nm. Although the photocycle was initially viewed as a series of sequential steps (13, 14), kinetic evidence suggests rapid equilibrium among the states within the 13-*cis* manifold (15–17). Excitation of photocycle intermediates generates off-pathway states, some of which have been reported to be fluorescent (18–21).

We previously speculated that voltage acted by modifying the protonation of the Schiff base in the ground state of Arch. However, illumination at 230 W/cm^2, typical for imaging, corresponds to $>10^4$ photon absorption events per molecule per second. Microbial rhodopsin photocycles typically last ∼10 ms. Thus, under photostationary imaging conditions, the ground state may be significantly depleted. Each photocycle intermediate has a different charge distribution, and thus the relative energy of intermediates depends on membrane voltage. A realistic model must acknowledge that fluorescence and voltage sensitivity could arise anywhere in the photocycle.

Early transient absorption measurements on BR in vesicles indicated that hyperpolarizing voltage slowed the decay of an M state (22–24). However, the membrane voltage was not precisely known in these experiments. Measurements of photocurrents in BR under patch-clamp conditions further indicated a voltage-dependent M-state decay (25–27). *Acetabularia* rhodopsin behaved similarly, but a differing kinetic model led to the conclusion that voltage primarily acted to slow the O-state decay (28).

Here, we combine patch-clamp measurements with fluorescence spectroscopy of Arch and its photogenerated intermediates (Fig. 1). In *Results*, *Optimization of Voltage Imaging*, we characterize the fluorescence, photocurrent, and voltage sensitivity spectra of Arch and the nonpumping mutant Arch(D95N) under steady-state illumination. This information enables straightforward optimization of imaging parameters and is intended for

Author contributions: D.M., V.V., H.L., and A.E.C. designed research; D.M., V.V., and H.L. performed research; D.M., V.V., and A.E.C. analyzed data; and D.M., V.V., and A.E.C. wrote the paper.

The authors declare no conflict of interest.

This article is a PNAS Direct Submission.

[1]D.M. and V.V. contributed equally to this work.

[2]To whom correspondence should be addressed. E-mail: cohen@chemistry.harvard.edu.

This article contains supporting information online at www.pnas.org/lookup/suppl/doi:10.1073/pnas.1215595110/-/DCSupplemental.

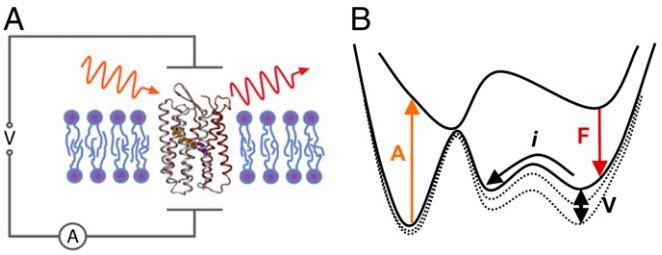

Fig. 1. Multimodal spectroscopy of a microbial rhodopsin. (*A*) Optical and electrical perturbations induce fluorescence and photocurrent responses. Rhodopsins have strong cross-modality couplings (illumination modulating current; voltage modulating fluorescence) as well as nonlinear optical and electrical responses. (*B*) Dynamics on a potential energy landscape. Absorption (A), fluorescence (F), and photocurrent (*i*) probe distinct types of transitions, whereas voltage modulates the shape of the landscape.

readers wishing to perform voltage-imaging experiments. In *Results*, *Photocycle of Arch*, we study the transient absorption and transient fluorescence of Arch to characterize the photocycle. In *Results*, *Optoelectronic Properties of Arch*, we combine optical with electrical measurements to probe cross-couplings between illumination and current, and between voltage and fluorescence. We conclude that fluorescence arises through a sequential three-photon process and that membrane voltage tips the relative balance of an *M*-like and an *N*-like intermediate.

Results

Optimization of Voltage Imaging. We sought to determine the illumination conditions (wavelength and intensity) most conducive to voltage imaging and least perturbative to membrane potential. The apparatus consisted of an inverted epifluorescence microscope equipped with multiple laser lines, combined with a patch-clamp electrophysiology rig (*SI Appendix*, Fig. S2). We expressed Arch in HEK293T cells and recorded fluorescence and photocurrent as a function of illumination wavelength, illumination intensity, and membrane voltage. All experiments were performed at 25 °C unless otherwise indicated.

Under steady-state high-intensity illumination (1,000 W/cm^2, 594 nm), Arch fluorescence increased by $\Delta F/F = 35\%$ between −150 and +150 mV [under 640-nm illumination, the sensitivity was $\Delta F/F = 100\%$ for the same voltage range (8)]. A fit to a Hill curve showed that the voltage-sensitive transition experienced a fraction $\alpha \sim 0.15$ of the total membrane voltage (*SI Appendix*). We used a photomultiplier to measure the fluorescence response to a step in applied voltage (Fig. 2*B*, and *SI Appendix*, Fig. S3). The membrane voltage lagged the applied voltage by ∼0.4 ms due to the *RC* charging time of the membrane. After accounting for this lag analytically, we found that the protein step response had a time constant of 0.6 ms (*SI Appendix*).

A puzzle in our initial experiments was the relative ease with which we imaged Arch in the microscope, compared with the reported extremely low fluorescence quantum yield (10^{-4}–10^{-3}) of all known microbial rhodopsins (20, 29, 30). The fluorescence of BR was reported to increase faster than linearly with increasing excitation intensity (31). We thus measured Arch fluorescence, *F*, as a function of illumination intensity, *I* [excitation (exc.), 532, 594, or 640 nm; emission (em.), 660–760 nm] in a sample of fractionated *Escherichia coli* membranes containing an Arch-eGFP fusion (Fig. 2*C*). Indeed, the relative brightness of Arch (*F*/*I*) increased at higher illumination intensity, growing 10-fold between 0.05 and 200 W/cm^2 (exc., 594 nm). In contrast, eGFP showed *F*/*I* independent of illumination intensity (exc., 488 nm; em., 511–551 nm). We previously reported that under dim illumination Arch was 500-fold dimmer than eGFP (8). Our present results show that, under intense illumination, Arch is only 50-fold dimmer than eGFP. We measured the photocurrent as a function of illumination intensity and observed saturation behavior: under intense illumination, additional light did not lead to additional photocurrent (*SI Appendix*, Fig. S4).

We visually demonstrated the nonlinear increase in Arch fluorescence with increasing illumination intensity in a cuvette of purified Arch-eGFP fusion protein. The cuvette was illuminated with focused continuous-wave (CW) illumination at 473 nm (2 μW, to excite eGFP) and 594 nm (5 μW, to excite Arch) (Fig. 2*D* and *SI Appendix*). Although eGFP fluoresced throughout the beam path, Arch fluoresced predominantly at the focus. This nonlinear increase in Arch fluorescence occurred at an intensity ∼10^{10}-fold lower than typically required for two-photon microscopy, implying a sequential multiphoton process in Arch, in contrast to the coherent multiphoton excitation commonly observed with pulsed femtosecond excitation.

We measured four key action spectra of Arch: photocurrent, ground-state absorbance, fluorescence excitation, and voltage sensitivity of fluorescence (*SI Appendix*). Due to the nonlinear dependence of Arch fluorescence on illumination intensity, we took care to maintain constant illumination intensity of 10 W/cm^2 across all wavelengths. Arch generated the largest photocurrent when excited at 530 nm (typically ∼40 pA), absorbed maximally at 552 nm (extinction coefficient 50,300 $M^{-1}\cdot cm^{-1}$; *SI Appendix*, Fig. S5), showed maximal fluorescence (*F*) when excited at 570 nm and exhibited maximal change in fluorescence (ΔF) upon a voltage step when excited at 590 nm. Due to the differing spectra of *F* and ΔF, the peak in the fractional voltage sensitivity, $\Delta F/F$, occurred at a different wavelength (640 nm; *SI Appendix*, Fig. S6*A*) than the peak in ΔF (590 nm; Fig. 2*E*). These differing spectra further indicate that optical excitation of multiple states is involved in determining the photoresponse of Arch.

These findings inform the choice of optics used to image Arch. To maximize voltage sensitivity and to minimize photocurrent, the illumination should be red or orange. Although green illumination produces comparatively strong fluorescence, this fluorescence is not sensitive to voltage. With conventional fluorophores one can trade exposure time for illumination intensity to maintain a constant signal. Due to the multiphoton excitation of Arch, this tradeoff is not possible. Illumination with a light-emitting diode or arc lamp produces barely detectable fluorescence, whereas intense illumination (typically from a laser) leads to a robust signal.

We previously introduced the mutant Arch(D95N) as a nonpumping voltage reporter. We characterized Arch(D95N) by the same measures as in Fig. 2 (*SI Appendix*, Fig. S7). This mutant had a slower response time than wild-type Arch, with a minor (∼20%) component occurring in <1 ms, and a major (∼80%) component lasting 36 ms rising, 30 ms falling at 25 °C. Remarkably, at 35 °C the fast component grew significantly, accounting for ∼55% of the response. These results will be useful to researchers interested in using Arch(D95N) as a voltage indicator. The fractional voltage sensitivity of wild-type Arch, $\Delta F/F$, was relatively insensitive to illumination intensity between 10 and 1,000 W/cm^2, whereas for Arch(D95N) $\Delta F/F$ increased threefold to fivefold over this range, depending on the excitation wavelength (*SI Appendix*, Fig. S6).

Photocycle of Arch. Transient absorption spectra of detergent-solubilized Arch were recorded with excitation by a nanosecond pulsed Nd:YAG laser at 532 nm (Fig. 3 *A* and *B*). These spectra closely matched corresponding spectra of Archaerhodopsin 1 (32) and BR (33). The pH-dependent transient absorption (Fig. 4*C*, below) suggested a slowing of *M* formation at pH 6, consistent with proton release preceding *M* formation. Formation of *O* was slower at pH 8, indicating that proton uptake preceded *O* formation. As with BR, Arch showed dark adaptation. When left in the dark for several minutes, Arch spontaneously converted into a state with increased initial fluorescence upon onset of illumination (*SI Appendix*, Fig. S8). In BR, dark adaptation corresponds to conversion from *all-trans* retinal to a mixture of *all-trans* and 13-*cis* retinal (34).

The ambiguities in inferring a kinetic model from transient absorption alone have been well documented (33, 35). Based on the strong sequence and spectroscopic homology between Arch and

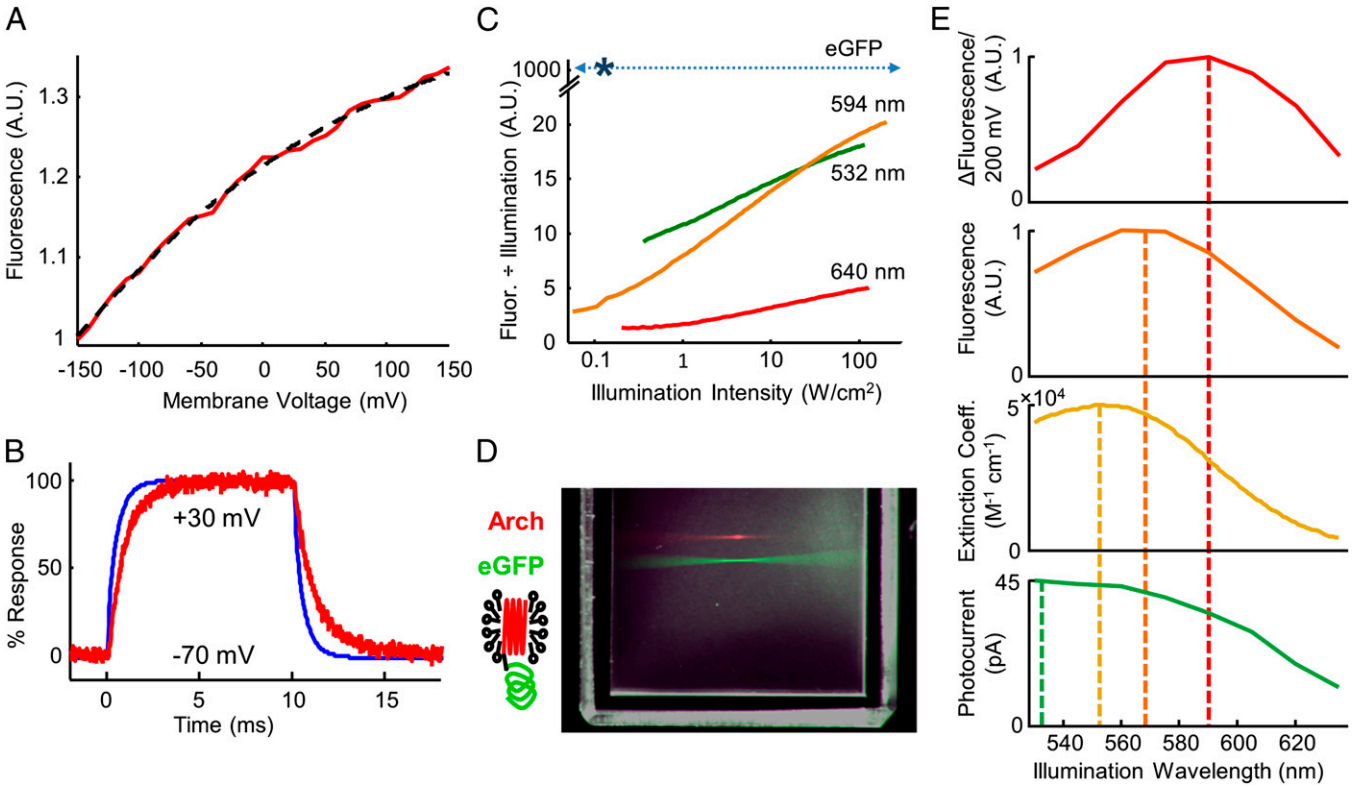

Fig. 2. Arch as a voltage indicator. (*A*) Voltage-sensitive fluorescence of Arch (exc., 594 nm; 1,000 W/cm^2; em., 660–760 nm). The dashed line is a fit to a two-state Boltzmann distribution (*SI Appendix*). (*B*) Fluorescence response (red) to a voltage step from −70 to +30 mV (blue). The time constant of the voltage step arose from capacitive charging of the membrane (*SI Appendix*). (*C*) Ratio of fluorescence to illumination intensity (*F*/*I*), as a function of illumination intensity. (*D*) Visual demonstration of nonlinear dependence of Arch fluorescence on CW illumination intensity. Two laser beams were focused inside a cuvette containing an Arch-eGFP fusion. The top beam (594 nm) excited fluorescence from Arch. The identically shaped bottom beam (473 nm) excited fluorescence from eGFP. Arch fluorescence was localized to the focus, whereas eGFP fluorescence occurred throughout the beam. Image is a pseudocolored composite of three exposures taken under different camera settings (*SI Appendix*). (*E*) Action spectra of Arch showing distinct spectra for different quantities.

BR, we assumed a BR-like photocycle and used the transient absorption data to infer rate constants. Fig. 3*B* shows the fit of this model to some of the transient absorption data. This model indicates that a blue-absorbing *M* state formed within 50 μs and decayed with a time constant of 390 μs. A red-absorbing *O* state arose with two time constants of 390 μs and 4.1 ms, and decayed with a time constant of 14 ms. The *N* state is not directly visible in the transient absorption due to its strong spectral overlap with the ground state. Fitting parameters are given in *SI Appendix*, Table S1.

To determine which intermediate state (or states) produced fluorescence, we performed transient fluorescence experiments on fractionated *E. coli* membranes containing Arch. An intense green pump pulse (50 W/cm^2, 100 μs, 532 nm) initiated the photocycle. A weak red probe pulse (15 W/cm^2, 100 μs, 640 nm) excited fluorescence with variable delay after the pump.

Illumination with the probe alone produced barely detectable fluorescence [Fig. 3*C*, (i)], consistent with the expected low fluorescence quantum yield of the Arch ground state. Application of a single pump pulse before the probe produced a species more than twice as fluorescent as the ground state. This species appeared in <20 μs and decayed with a time constant of 1.0 ms [Fig. 3*C*, (ii)]. Remarkably, application of two pump pulses before the probe [timing shown in Fig. 3*C*, (iii)] produced up to sixfold more fluorescence than the ground state. Fluorescence peaked with an interval of 10 ms between the pump pulses [Fig. 3*C*, (iii)]. These experiments established that the fluorescence of Arch arises from a sequential three-photon process: one photon to initiate the photocycle, a second to generate the fluorescent species from a photointermediate, and a third photon to induce fluorescence.

We characterized the action spectra and saturation properties of each of the three photons (*SI Appendix*, Figs. S9–S11). Photon 1 matched the ground-state absorption spectrum of Arch. Photon 2 was blue-shifted by 10 nm relative to photon 1. In BR, the *N* state has a 10-nm blue shift relative to the ground state, so we provisionally assign photon 2 to excitation of an *N*-like intermediate. Photon 3 peaked at 570 nm. At low intensities of pumps 1 and 2, the fluorescence from pump 3 was linear in all three pump intensities, confirming that each contributed a single photon. We also measured the spontaneous decay (presumably back to *N*) of the fluorescent state, and found a time constant of 0.84 ms. We combined the transient absorption and fluorescence data to propose a photocycle shown in Fig. 3*D*.

Ohtani and coworkers (20, 31, 36) found that in BR sequential absorption of two photons generated a state, termed *Q*, which could be excited by a third photon to yield fluorescence. [The term "*Q*" state has been used to represent other intermediates in the BR photocycle (18). Here, we refer exclusively to the Ohtani *Q*.] This state had an excited state lifetime of 62 ps, vs. ∼500 fs for the ground state, and was thus ∼100-fold more fluorescent than the ground state (36). The *Q* state was excited by red light and emitted in the near infrared with a peak at ∼720 nm. The timing in the photocycle, excitation and emission spectra, and thermal relaxation rate of our fluorescent state match the Ohtani *Q* state, so we designate the dominant fluorescent state *Q*.

The complex photophysics of Arch fluorescence have important implications for its use as a fluorescent label in confocal microscopy. During a frame-scanning confocal measurement, each molecule experiences microsecond bursts of intense illumination, spaced by hundreds of milliseconds of darkness. These bursts are shorter than the time required for Arch to enter the

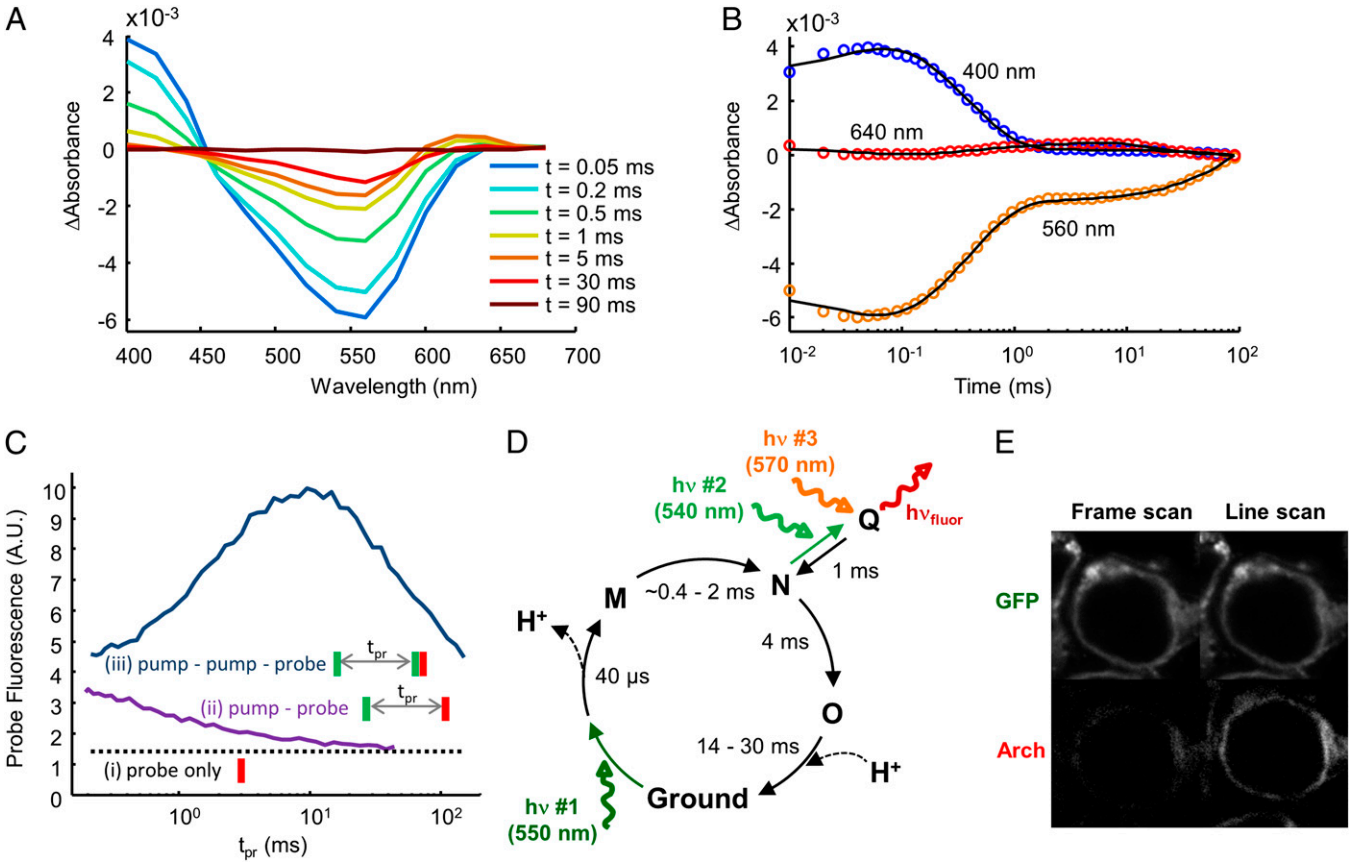

Fig. 3. Time-resolved spectroscopy of Arch. (*A*) Transient absorption spectra showing early rise of a blue-shifted *M* intermediate, and late rise of a red-shifted *O* intermediate. (*B*) Time-dependent absorption data are well described by a fit to four exponential decays. (*C*) Transient fluorescence experiments established that fluorescence was dominated by a sequential three-photon process. (*D*) Proposed photocycle with rates derived from transient absorption and transient fluorescence data. (*E*) Confocal scans showing the effects of scan speed on brightness. Arch fluorescence was sensitive to the timing of the illumination, whereas eGFP fluorescence was not.

fluorescent Q state, and the interburst interval is longer than the photocycle. Thus, under frame-scanning conditions, Arch appeared very dim (Fig. 3*E*). In line-scanning mode, each line of the image was scanned multiple times before the laser advanced to the next line. The interval between line scans (~0.5 ms) was shorter than the photocycle, so the illumination in each scan sensitized fluorescence in subsequent scans. Arch then appeared brighter. In an Arch-eGFP fusion, the brightness of eGFP was independent of the scan mode.

Optoelectronic Properties of Arch. To identify states whose population depended on voltage, we transiently expressed Arch in HEK293T cells, and recorded membrane current $i(t)$ and fluorescence $F(t)$ as functions of the membrane voltage $V_m(t)$ and illumination $I(\lambda,t)$. Three attributes of voltage-sensitive fluorescence were immediately striking: (*i*) A step in illumination (from darkness) under constant voltage induced fluorescence that was initially not sensitive to membrane voltage (Fig. 4*A*). Fluorescence became sensitive to voltage with a time constant of 2 ms. (*ii*) A step in voltage under constant illumination induced a fluorescence response with a time constant of 0.6 ms (Fig. 2*A*). (*iii*) An initial flash of light sensitized the protein so that fluorescence from a second flash was (*a*) brighter than fluorescence from an isolated flash, and (*b*) sensitive to voltage (Fig. 4*B*). Both forms of sensitization arose with a time constant of 2 ms and fell with a time constant of 30 ms.

Observation (*i*) rules out a voltage-dependent change in the ground state as the origin of voltage-dependent fluorescence, in contrast to our previously proposed model (8). Observation (*ii*) requires that the voltage-sensitive step be fast, and either involve the fluorescent state directly, or be coupled to the fluorescent state by fast rate constants. Observation (*iii*) establishes that the voltage-sensitive manifold is long lasting. Thus, the fast voltage-sensitive rate is preceded by a somewhat slower step and is followed by a much slower step in the photocycle.

Two other measurements pointed to a long-lived voltage-sensitive intermediate. In a double-flash experiment, the photocurrent from the second flash was smaller than from the first, recovering with a time constant of 32 ms (a two-exponential fit yielded time constants of 3.8 and 54 ms; *SI Appendix*, Fig. S12). The photocurrent recovery reflects ground-state repopulation and thus indicates a long-lived intermediate.

We performed an electrical test for a voltage-dependent equilibrium in this long-lived intermediate by measuring membrane capacitance as a function of time after a single flash (*SI Appendix*, Fig. S14). A voltage-dependent chemical equilibrium must increase membrane capacitance through the voltage-dependent charge redistribution. We observed a flash-induced increase in membrane capacitance that recovered on a 30-ms timescale (Fig. 4*B*). The maximum light-induced change in capacitance was $\delta C = 0.1$ pF, on a baseline membrane capacitance of $C = 41$ pF. Although the transient capacitance provides mechanistic insight, its magnitude $\delta C/C = 0.25\%$ suggests that light-induced capacitive loading is negligible.

By fitting the amplitude of the transient capacitance to a two-state model at thermal equilibrium (*SI Appendix*), we inferred that the relative energies of the two states in voltage-dependent equilibrium were shifted by an energy αV_m, with $\alpha = 0.1$. This value is in reasonable agreement with the value $\alpha = 0.15$ extracted from a fit of a Hill curve to the plot of F vs. V_m (Fig. 2*A*).

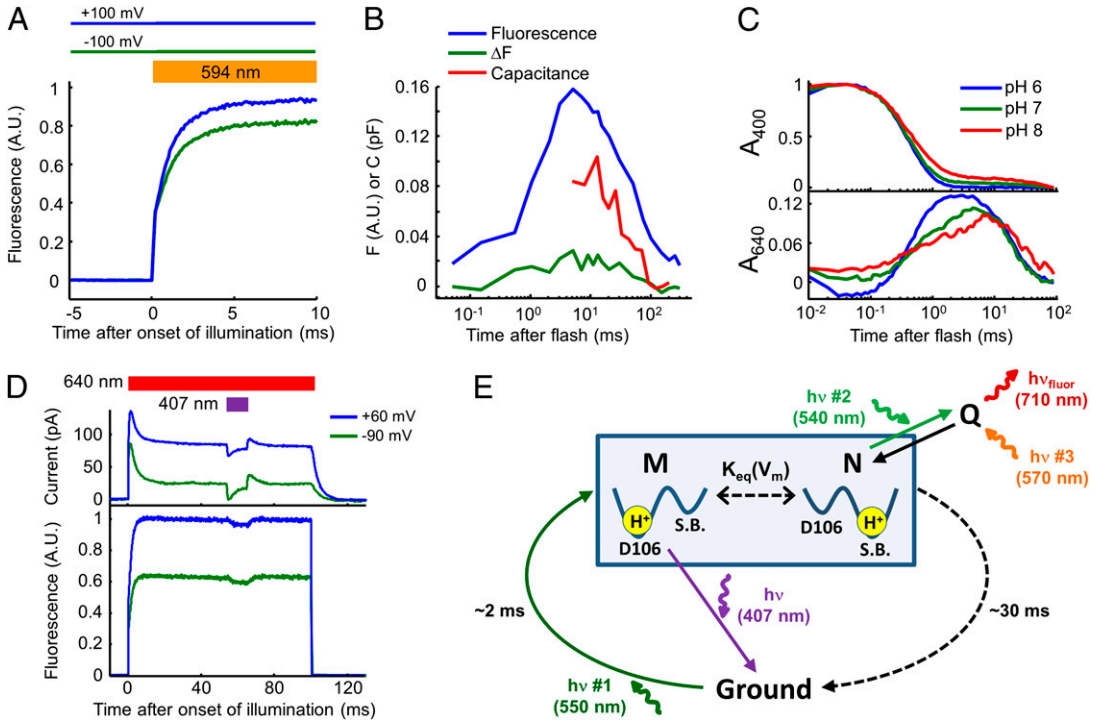

Fig. 4. Optoelectronic dynamics of Arch. (*A*) Fluorescence response of Arch to a step in illumination at V_m = +100 and −100 mV. (*B*) Transient responses of Arch in a double-flash experiment. Fluorescence from the second flash rose and fell following initiation of the photocycle. The difference in fluorescence between +30 and −70 mV, Δ*F*, rose and fell with the fluorescence. A single flash induced a similar trajectory of membrane capacitance. (*C*) Transient absorption in solubilized Arch as a function of pH, normalized to the maximum signal at 400 nm. (*D*) Photocurrent and fluorescence in response to illumination with a pulse of red light, with a superimposed pulse of violet light. (*E*) A simplified model of voltage sensitivity and fluorescence in Arch. Photon #1 initiates the photocycle. Voltage modulates a proton-transfer equilibrium between two photocycle intermediates: an *M* state with a protonated donor (D106) and an *N* state with a protonated Schiff base (S.B.). Fluorescence arises through conversion of *N* to *Q* (photon #2) followed by electronic excitation of *Q* (photon #3).

The local access model of the BR photocycle proposes that all 13-*cis* photointermediates—*L*, M_1, M_2, and *N*—are in rapid equilibrium (16). Fluorescence arises from a branch off *N*, so we hypothesized that voltage acted within the 13-*cis* manifold. We further hypothesized that voltage acted by modulating the protonation of a fluorescence-determining functional group within the 13-*cis* manifold. Thus, a state whose population showed pH sensitivity near neutral pH would be a plausible voltage-sensitive state. We performed transient absorption spectroscopy on detergent-solubilized Arch as a function of pH. At pH 8, a long-lived *M* state appeared (Fig. 4*C*).

Based on the pH-dependent transient absorption, and the extensive literature suggesting a voltage-dependent *M* decay in BR, we tested whether membrane voltage tuned an $M \rightleftharpoons N$ equilibrium in Arch. This hypothesis was attractive because (*a*) an *M* state would not be excited by the red or orange laser, and thus could be a dark equilibrium partner with the prefluorescent *N* state; and (*b*) in the $M \rightarrow N$ transition, the Schiff base is reprotonated from the proton donor (D106), which resides between the Schiff base and the cytoplasm. The long range (10.5 Å in BR) and orientation of this proton-transfer would favor the nonfluorescent *M* state at negative voltage and the prefluorescent *N* state at positive voltage, consistent with the observed dependence of fluorescence on voltage.

To test this hypothesis, we used flashes of violet light (407 nm) to depopulate the *M* state under photostationary red light illumination. Violet light is known to induce 13-*cis* to *all-trans* isomerization in the *M* state, short-circuiting the photocycle from *M* to ground. Similar illumination protocols have been used in BR (25, 26) and in *Acetablularia* rhodopsin (28). We recorded the photocurrent and fluorescence under red and (red plus violet) illumination, as a function of membrane voltage.

Under photostationary red illumination, addition of violet light decreased the photocurrent and the fluorescence, indicating the presence of an *M*-state population (Fig. 4*D*). To test whether these data were consistent with a voltage-dependent $M \rightleftharpoons N$ equilibrium, we constructed a highly simplified model of the photocycle shown in Fig. 4*E*. The $M \rightleftharpoons N$ interconversion was assumed to be fast compared with the other rates, and thus always at equilibrium. Red illumination delivered population into the 13-*cis* manifold, while molecules relaxed back to ground at a rate proportional to the *N* population. Violet illumination introduced an additional relaxation pathway, with a rate proportional to the *M* population.

This model quantitatively reproduced (*a*) the shapes of the photocurrent and fluorescence transients upon onset of red illumination; (*b*) the dependence of steady-state fluorescence and photocurrent on membrane voltage under red illumination only; and (*c*) the effect of violet illumination on fluorescence and photocurrent (*SI Appendix*, Fig. S13). We thus conclude that a voltage-dependent $M \rightleftharpoons N$ equilibrium is a likely explanation for voltage-dependent fluorescence in Arch.

Due to the small number of states, the model could not reproduce the complex kinetics of ground-state recovery. This model does not rule out more complex mechanisms of voltage sensitivity, such as voltage-dependent equilibria among *L*, M_1, and M_2, or multiple voltage-dependent rates. Our data do not distinguish between these scenarios.

Discussion

The ground state of Arch is only weakly fluorescent, but a photogenerated intermediate is roughly 10-fold brighter than previously thought. Fluorescence arises through sequential action of three photons. Voltage sensitivity is a property of a 13-*cis* photocycle intermediate, not the ground state, and likely arises

through protonation of the Schiff base from the cytoplasmic side (i.e., a voltage-dependent $M \rightleftharpoons N$ equilibrium). The free energy of this reaction has a component equal to αV_m, with $\alpha \sim 0.15$; or in the language of electrophysiology, the gating charge is ~0.15 e. Many fluorescent voltage indicators significantly increase membrane capacitance, leading to electrical loading of the cell. Arch only acts as a voltage sensor in a photocycle intermediate, and in this intermediate the fractional increase in membrane capacitance is $\delta C/C < 1\%$.

A clear strategy for increasing the voltage sensitivity and brightness of Arch is to generate a protein with a 13-*cis* ground state or a metastable 13-*cis* intermediate. For instance, the D96N and D96N/D115N mutations of BR are known to prolong the lifetime in the 13-*cis* manifold (37), so homologous mutations in Arch (D106N, D125N) may enable voltage imaging under lower illumination intensities.

We further propose that mutations on the extracellular side designed to block current (such as D95N in Arch) are more likely to preserve voltage sensitivity than are mutations on the cytoplasmic side. The fluorescent *Q* state is reached by photoexcitation of the 13-*cis N* state. Thus, *Q* is unlikely to be exclusively 13-*cis*, but its isomerization state is not known. A structural model of *Q* would facilitate efforts to engineer proteins with improved brightness.

The differing spectra of *F* and ΔF (Fig. 2*E*), and the presence of fluorescence immediately upon illumination (Figs. 3*C* and 4*A*) indicate that the photocycle may contain two (or more) fluorescent species, not all of which are voltage sensitive. Our study has focused on the dominant voltage-sensitive species. The other fluorescent state(s) await characterization. Furthermore, under simultaneous illumination at two wavelengths within the visible (530–640 nm) the fluorescence and photocurrent depended in a complex way on the wavelengths and relative intensities of the illumination (*SI Appendix*, Fig. S15). These effects likely arise from additional light-driven pathways not included in our simple models.

The rich spectroscopic and optoelectronic properties of microbial rhodopsins have previously been considered for application in optical information processing and data storage (38). Although such applications have not yet been widely adopted, the ability of rhodopsins to transduce light into changes in membrane voltage have enabled many optogenetic tools. We propose that optoelectronic coupling in the opposite direction—changes in membrane voltage affecting optical properties—will enable a similarly broad set of applications in bioimaging.

Materials and Methods

Transient absorption experiments were performed on purified protein in a homemade transient absorption spectrometer. All other experiments were performed on a homemade inverted fluorescence microscope, equipped with time-gated illumination at multiple wavelengths, time-resolved detection, and a patch-clamp electrophysiology rig. HEK293T cells were grown following standard protocols and transiently transfected with the gene of interest. Cells were subjected to time-varying illumination and time-varying membrane voltage, and the ensuing fluorescence and membrane current were digitized and recorded. Details are provided in *SI Appendix*.

ACKNOWLEDGMENTS. We thank Joel Kralj, Daniel Hochbaum, Jeehae Park, and Lucy Rosenbaum for discussions and assistance with tissue culture. This work was supported by Presidential Early Career Award for Scientists and Engineers Award N00014-11-1-0549, the Harvard Center for Brain Science, National Institutes of Health (NIH) Grants 1-R01-EB012498-01 and New Innovator Grant 1-DP2-OD007428, the Harvard/Massachusetts Institute of Technology Joint Research Grants Program in Basic Neuroscience, a Herchel Smith Graduate Fellowship (to V.V.), NIH Medical Scientist Training Program Grant T32GM07753-33 (to V.V.), and a Frank Knox Memorial Fellowship (to D.M.).

1. Scanziani M, Häusser M (2009) Electrophysiology in the age of light. *Nature* 461(7266):930–939.
2. Peterka DS, Takahashi H, Yuste R (2011) Imaging voltage in neurons. *Neuron* 69(1):9–21.
3. Kaestner L, Tian Q, Lipp P (2012) Action potentials in heart cells. *Fluorescent Proteins II*, ed Jung G (Springer, Berlin), pp 163–182.
4. Adams DS, Masi A, Levin M (2007) H^+ pump-dependent changes in membrane voltage are an early mechanism necessary and sufficient to induce *Xenopus* tail regeneration. *Development* 134(7):1323–1335.
5. Martinac B, Saimi Y, Kung C (2008) Ion channels in microbes. *Physiol Rev* 88(4):1449–1490.
6. Cohen LB, Keynes RD, Hille B (1968) Light scattering and birefringence changes during nerve activity. *Nature* 218(5140):438–441.
7. Tasaki I, Watanabe A, Sandlin R, Carnay L (1968) Changes in fluorescence, turbidity, and birefringence associated with nerve excitation. *Proc Natl Acad Sci USA* 61(3):883–888.
8. Kralj JM, Douglass AD, Hochbaum DR, Maclaurin D, Cohen AE (2012) Optical recording of action potentials in mammalian neurons using a microbial rhodopsin. *Nat Methods* 9(1):90–95.
9. Kralj JM, Hochbaum DR, Douglass AD, Cohen AE (2011) Electrical spiking in *Escherichia coli* probed with a fluorescent voltage-indicating protein. *Science* 333(6040):345–348.
10. Chattoraj M, King BA, Bublitz GU, Boxer SG (1996) Ultra-fast excited state dynamics in green fluorescent protein: Multiple states and proton transfer. *Proc Natl Acad Sci USA* 93(16):8362–8367.
11. Ihara K, et al. (1999) Evolution of the archaeal rhodopsins: Evolution rate changes by gene duplication and functional differentiation. *J Mol Biol* 285(1):163–174.
12. Chow BY, et al. (2010) High-performance genetically targetable optical neural silencing by light-driven proton pumps. *Nature* 463(7277):98–102.
13. Váró G, Lanyi JK (1991) Thermodynamics and energy coupling in the bacteriorhodopsin photocycle. *Biochemistry* 30(20):5016–5022.
14. Váró G, Lanyi JK (1991) Kinetic and spectroscopic evidence for an irreversible step between deprotonation and reprotonation of the Schiff base in the bacteriorhodopsin photocycle. *Biochemistry* 30(20):5008–5015.
15. Spudich JL, Yang CS, Jung KH, Spudich EN (2000) Retinylidene proteins: Structures and functions from archaea to humans. *Annu Rev Cell Dev Biol* 16:365–392.
16. Brown LS, Dioumaev AK, Needleman R, Lanyi JK (1998) Local-access model for proton transfer in bacteriorhodopsin. *Biochemistry* 37(11):3982–3993.
17. Brown LS, Dioumaev AK, Needleman R, Lanyi JK (1998) Connectivity of the retinal Schiff base to Asp85 and Asp96 during the bacteriorhodopsin photocycle: The local-access model. *Biophys J* 75(3):1455–1465.
18. Popp A, Wolperdinger M, Hampp N, Brüchle C, Oesterhelt D (1993) Photochemical conversion of the O-intermediate to 9-*cis*-retinal-containing products in bacteriorhodopsin films. *Biophys J* 65(4):1449–1459.
19. Yamamoto N, Naramoto S, Ohtani H (1992) Photoreaction of N560 intermediate in the photocycle of bacteriorhodopsin. *FEBS Lett* 314(3):345–347.
20. Ohtani H, Itoh H, Shinmura T (1992) Time-resolved fluorometry of purple membrane of *Halobacterium halobium*. O640 and an O-like red-shifted intermediate Q. *FEBS Lett* 305(1):6–8.
21. Ohtani H, Kikuchi O (1999) Excitation spectrum of the N intermediate in the photocycle of bacteriorhodopsin. *J Phys Chem B* 103(38):8186–8188.
22. Dancshazy Z, Helgerson S, Stoeckenius W (1983) Coupling between the bacteriorhodopsin photocycle kinetics and the protonmotive force. I. Single flash measurements in *Halobacterium halobium* cells. *Photobiochem Photobiophys* 5:347–357.
23. Groma GI, et al. (1984) Coupling between the bacteriorhodopsin photocycle and the protonmotive force in *Halobacterium halobium* cell envelope vesicles. II. Quantitation and preliminary modeling of the M →bR reactions. *Biophys J* 45(5):985–992.
24. Quintanilha AT (1980) Control of the photocycle in bacteriorhodopsin by electrochemical gradients. *FEBS Lett* 117(1):8–12.
25. Geibel S, et al. (2001) The voltage-dependent proton pumping in bacteriorhodopsin is characterized by optoelectric behavior. *Biophys J* 81(4):2059–2068.
26. Nagel G, Kelety B, Möckel B, Büldt G, Bamberg E (1998) Voltage dependence of proton pumping by bacteriorhodopsin is regulated by the voltage-sensitive ratio of M1 to M2. *Biophys J* 74(1):403–412.
27. del Rosario RCH, Oppawsky C, Tittor J, Oesterhelt D (2010) Modeling the membrane potential generation of bacteriorhodopsin. *Math Biosci* 225(1):68–80.
28. Tsunoda SP, et al. (2006) H^+-pumping rhodopsin from the marine alga *Acetabularia*. *Biophys J* 91(4):1471–1479.
29. Bogomolni RA, Stubbs L, Lanyi JK (1978) Illumination-dependent changes in the intrinsic fluorescence of bacteriorhodopsin. *Biochemistry* 17(6):1037–1041.
30. Du M, Fleming GR (1993) Femtosecond time-resolved fluorescence spectroscopy of bacteriorhodopsin: Direct observation of excited state dynamics in the primary step of the proton pump cycle. *Biophys Chem* 48(2):101–111.
31. Kamiya N, et al. (1997) Picosecond fluorescence spectroscopy of the purple membrane of *Halobacterium halobium* in alkaline suspension. *Chem Phys Lett* 265(6):595–599.
32. Mukohata Y, Ihara K, Uegaki K, Miyashita Y, Sugiyama Y (1991) Australian Halobacteria and their retinal-protein ion pumps. *Photochem Photobiol* 54(6):1039–1045.
33. Ludmann K, Gergely C, Váró G (1998) Kinetic and thermodynamic study of the bacteriorhodopsin photocycle over a wide pH range. *Biophys J* 75(6):3110–3119.
34. Scherrer P, Mathew MK, Sperling W, Stoeckenius W (1989) Retinal isomer ratio in dark-adapted purple membrane and bacteriorhodopsin monomers. *Biochemistry* 28(2):829–834.
35. Stoeckenius W, Bogomolni RA (1982) Bacteriorhodopsin and related pigments of halobacteria. *Annu Rev Biochem* 51:587–616.
36. Ohtani H, Kaneko M, Ishikawa M, Kamiya N, Yamamoto N (1999) Picosecond-millisecond dual-time-base spectroscopy of fluorescent photointermediates formed in the purple membrane of *Halobacterium halobium*. *Chem Phys Lett* 299(6):571–575.
37. Zimányi L, et al. (1992) Pathways of proton release in the bacteriorhodopsin photocycle. *Biochemistry* 31(36):8535–8543.
38. Hillebrecht JR, et al. (2005) Optimization of protein-based volumetric optical memories and associative processors by using directed evolution. *NanoBiotechnology* 1:141–151.